# Bending properties of Ag nanowires with pre-existing surface defects

*H F Zhan, Y T Gu*, C Yan and P K.D.V. Yarlagadda*

*School of Chemistry, Physics and Mechanical Engineering, Queensland University of Technology, Brisbane 4001, Australia*

***Corresponding Author:** Dr. Yuantong Gu

**Mailing Address:** School of Chemistry, Physics and Mechanical Engineering,

Queensland University of Technology,

GPO Box 2434, Brisbane, QLD 4001, Australia

**Telephones:** +61-7-31381009

**Fax:** +61-7-31381469

**E-mail:** yuantong.gu@qut.edu.au

**Abstract:** Materials used in the engineering always contain imperfections or defects which significantly affect their performances. Based on the large-scale molecular dynamics simulation and the Euler-Bernoulli beam theory, the influence from different pre-existing surface defects on the bending properties of Ag nanowires (NWs) is studied in this paper. It is found that the nonlinear-elastic deformation, as well as the flexural rigidity of the NW is insensitive to different surface defects for the studied defects in this paper. On the contrary, an evident decrease of the yield strength is observed due to the existence of defects. In-depth inspection of the deformation process reveals that, at the onset of plastic deformation, dislocation embryos initiate from the locations of surface defects, and the plastic deformation is dominated by the nucleation and propagation of partial dislocations under the considered temperature. Particularly, the generation of stair-rod partial dislocations and Lomer-Cottrell lock are normally observed for both perfect and defected NWs. The generation of these structures has thwarted attempts of the NW to an early yielding, which leads to the phenomenon that more defects does not necessarily mean a lower critical force.

**Keywords:** surface defect, bending, nanowire, beam theory, molecular dynamics

## 1. Introduction

Driven by their intriguing mechanical, electrical, optical, and other properties, nanowires (NWs) have drawn considerable interests from the scientific community. Their novel properties have enabled them being widely applied as building blocks of nanoelectromechanical systems (NEMS), such as high frequency resonator [1, 2], force and pressure sensing [3], ultrahigh-resolution mass sensing [4], and other devices [5]. In the past decade, increasing research efforts have been attributed for the better understanding of the mechanical performance of NWs. For instance, through *in situ* tensile experiments, Yue et al. [6] found Cu NWs could sustain ultrahigh elastic strains, and the defect-free Au NWs are reported showing superplasticity [7]. The size effects on elasticity, yielding, and fracture of five-fold twinned Ag NWs have been studied [8], and Richter et al. [9] confirmed that the properties of nanomaterials can be engineered by controlling defect and flaw densities. Various numerical studies including *ab initio* calculation, multi-scale simulation and molecular dynamics (MD) simulation have also been widely employed to investigate the performance of NWs, among which, the MD simulation is the most frequently applied method. A plenty of MD studies of the properties or performance of NWs can be found, which covers diverse loading conditions, including tension [10-12], compression or buckling [13], torsion [14], bending [15, 16], and vibration or resonance [17-19]. It is convinced that MD simulation is an effective and excellent tool, not only for the characterization of the properties of NWs, but also for the prediction of novel or unexpected properties.

Materials used in the real engineering always contain imperfections, which might be induced during the fabrication or manufacturing processes, e.g. impurity, grain boundaries (GBs), surface defects, nano-cavities and others [20]. Recent work conducted by Sansoz et al. [21] revealed that, twin boundaries (TBs) are ubiquitous for both synthesis and properties in nano-enhanced FCC metals. By using MD simulations, Chen et al. [22] reported that, during the machining and stretching of single crystal Cu, stacking faults (SFs) will be generated inside the specimen, which will greatly affect the specimen's properties under tension. Kuramoto et al. [23] investigated the fundamental behaviors of point defects, clusters and interaction with dislocation in Fe and Ni crystal by computer simulation. Besides of loading conditions and morphologies, Zhang et al. [24] reported that the strength of NWs also depends on the twin spacing. Experimental study [25] demonstrates that, NW mechanical properties could be uniquely tailored by controlling their structure (through assembling materials with oriented, interlocking grains). Apparently, due to the ultra small scale, the presence of defects behaviors as one of the most influential factors in determining NWs' properties. Thus, investigating the defect effect is crucial to enhance the utility of NWs. Several studies investigating the influence of pre-existing defects on the mechanical properties of NWs under tension [26], torsion [27], and others [28] have already been reported. However, the impacts from defects on the bending properties of NWs are still unclear, which becomes the object of this work.

Generally, a first ever investigation of the influence from pre-existing surface defects on the bending properties of NWs will be carried out in this paper. The Ag NW, which is popularly examined in experiments, will be chosen as the testing sample. Large-scale MD simulation will be employed to carry out the bending deformation, basing on the recently developed three-point bending model [16]. Pre-existing surface defects with different quantities, orientations, and locations will be investigated thoroughly. A comprehensive discussion of the mechanical properties including flexural rigidity, yield strength, and deformation configurations of different defected NWs will be made. To achieve this, both the classical Euler-Bernoulli beam model and the modified Euler-Bernoulli beam model augmented with a comprehensive consideration of surface/intrinsic effect and axial extension effect will be employed.

## 2. Numerical and theoretical basics

### *2.1 Molecular dynamics setting*

The study was conducted by large-scale MD simulations on doubly clamped Ag NWs subjected to bending deformation using LAMMPS [29]. Square cross-section Ag NW was considered with the $x$, $y$ and $z$ coordinate axes represent the lattice directions of $[100]$, $[010]$ and $[001]$, respectively. No periodic boundary condition was adopted. The simulation model is schematically shown in Fig. 1, which was established according to the AFM-bending method proposed by Wu et al. [25, 30].

Specifically, the bending is achieved by applying a constant velocity (1 m/s) to the cylindrical diamond tip, as shown in Fig. 1. To note that, loading rate exerts critical influence to the bending behaviors of NWs, and a velocity smaller than 10 m/s is recommended according to previous work [16]. The embedded-atom-method (EAM) potential [31] was used to describe the Ag-Ag atomic interactions, which was fitted to a group of parameters, including cohesive energy, equilibrium lattice constant, bulk modulus, and others [32]. For the Ag-C atomic interactions, a Morse potential [33] was adopted. During each simulation, NWs were first relaxed to a minimum energy state using the conjugate gradient energy minimization and then the Nose-Hoover thermostat [34, 35] was employed to equilibrate the NW at 0.01 K under canonical (NVT) ensemble. A time step of 2 fs was applied. To recognize the partial dislocation and stacking fault (SF) during the bending deformation, the centro-symmetry parameter (*CSP*) was adopted [36], which is defined by

$$CSP = \sum_{i=1,6} \left| \boldsymbol{R}_i + \boldsymbol{R}_{i+6} \right|^2 \tag{1}$$

where $\boldsymbol{R}_i$ and $\boldsymbol{R}_{i+6}$ are vectors corresponding to the six pairs of opposite nearest neighbors in FCC lattice. The *CSP* value increases from zero for perfect FCC lattice to positive values for defects and for atoms close to free surfaces.

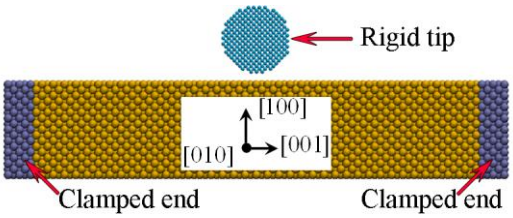


**Fig. 1.** The three-point bending simulation model. The two boundary regions are fixed in all directions to mimic the clamped end condition, with the rest as the deformation region. A rigid diamond cylindrical tip is employed, with the initial distance between the tip and NW as one Ag lattice constant. The diameter and length of the tip are 2.454 nm and 8.18 nm, respectively.

For each simulation, the size of the NW was uniformly chosen as $12a \times 12a \times 184a$, $a$ is the Ag lattice constant, which equals 0.409 nm [31]. As two lattice constants length was fixed as boundary regions at two ends, hence, the effective length is $180a$. The considered pre-existing surface defects were similar to the surface notch investigated by Doyama [37] and Tyagi et al. [38], or the defect of vacancies studied by Chang [39], which are schematically illustrated in Fig. 2. Different defects were introduced to the NW by removing certain number of atoms from the surface. For discussion convenience, the defect's quantity is referred by the fraction $dq=n/N$, where $n$ is the row number of the removed atoms, and $N$ is the total row number of the atoms in the lateral direction for a prefect atomic layer. For the NW considered in this work, $N$ equals 361. The orientation of the defect is defined according to its relative position with the NW's axial direction, and capital letters 'H', 'V', 'T' and 'E' denote horizontal, vertical, tilt (45°) and edge defects, respectively. According to this convention, all studied defects are summarized in Table 1.

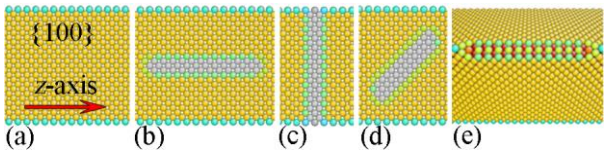


**Fig. 2.** Schematics of different surface defects. (a) A perfect (100) atomic layer; (b) Surface layer with vertical defect *dq*-V=3/361; (c) Surface layer with horizontal defect *dq*-H=3/361; (d) Surface layer with tilt defect *dq*-T=3/361; (e) Surface layers with edge defect *dq*-E=3/361. Gray atoms refer to the removed atoms.

**Table 1.** Summary of the testing models.

| Location | Bottom surface | | | | | | | | | Side & Top surfaces | | |
|---|---|---|---|---|---|---|---|---|---|---|---|---|
| Orientation | *dq*-H | | | | | | *dq*-V | *dq*-T | *dq*-E | *dq*-V | *dq*-T | *dq*-E |
| Quantity (1/361) | 1 | 3 | 5 | 7 | 9 | 11 | 3 | 3 | 3 | 3 | 3 | 3 |

*2.2 Theoretical basics*

Apparently, the NW studied in current work can be simplified as a doubly clamped thin beam bended by a central load $F$ (with the size denoted as $h \times h \times L$). According to the classical Euler-Bernoulli beam theory (shorted as EBT-Classical) [40], the beam maximum displacement $d$ and the applied load $F$ is described by

$$F = \frac{192EI}{L^3} d \tag{2}$$

where $EI$ is the flexural rigidity, and $L$ is the beam length. Obviously, equation (2) demonstrates a linear relationship between $F$ and $d$ for a given NW. It is known that when a beam is displaced, an axial tensile force is inherently induced due to the stretching. Results from both experiments [41] and MD simulations [16] suggest that, when the size is down to nano-scale, such stretching force exerts significant influence to the NW's bending behaviors and the $F$-$d$ curve becomes increasingly nonlinear as the displacement passes one cross-section size $h$. Furthermore, due to the extreme large aspect ratio, the surface stress also exerts remarkable influence to the properties of NWs. Several novel surface-driven mechanical behaviors and properties of NWs such as phase transformations [42, 43], pseudoelastic behavior [44], and shape memory effect [32, 45] have been reported. Recently, Liang et al. [46] found that the nonlinear elasticity of NW core plays a considerably large role in determining the elastic modulus of NWs subjected to uniaxial loads. Other researchers also reported that, the magnitude of the residual intrinsic stress induced by the residual surface stress is on the order of MPa to GPa in NWs [47]. In consideration of these factors, the classical beam model is augmented with the contributions from surface stress, intrinsic stress, as well as the axial extension effect by Zhan and Gu [48], predictions from which agrees well with the MD results. Specifically, this modified beam model (referred as EBT-ASI) gives a nonlinear relationship between $F$ and $d$ as [48]

$$F = \frac{192(EI)^*}{L^3} d\left(1 + \frac{\mu HL^2}{48(EI)^*} + \frac{(EA)^* + 2\mu E_s h}{24(EI)^*} d^2\right) \quad (3)$$

where $(EI)^*=Eh^4/12+2E_sh/3$ and $(EA)^*=EA+4E_sh$, which are the effective flexural rigidity [49] and the effective extensional rigidity [50], respectively. Here, $E_s$ is the surface Young's modulus, which equals 1.22 N/m for the {100} Ag surface [51]. $A$ and $h$ are the cross-sectional area and size, respectively. $\mu$ is a constant, and chosen as 0.25 for Ag NW [48]. Meanwhile, the yield strength can be deduced from the *F-d* curves according to [40]

$$Y = 3F_y L / (4h^3) \quad (4)$$

where $F_y$ is the yield force or critical force.

## 3. Results and discussion

### *3.1. Influence of defect's quantity*

Firstly, six Ag NWs with different quantities of horizontal defects that located at the bottom surface are considered. As seen in Fig. 3(a), comparing with the perfect NW, all defected NWs appear a coincident portion of the *F-d* curve before the onset of the plastic deformation or yielding. However, an apparent decrease of the critical force is observed due to the existence of defects (the critical force refers the force when the NW enters plastic deformation). The most striking finding is that the increase of the defect's quantity does not actually lead to the increase of the critical force reduction. For instance, the critical forces are around 23 nN and 23.6 nN for *dq*-H=3/361 and *dq*-H=7/361, respectively. To explore the mechanisms behind this phenomenon, the atomic configurations of NWs at different displacements will be investigated in the following context.

Fig. 3(b) shows the comparisons between MD results and fitting results from both EBT-Classical and EBT-ASI for the NW with *dq*-H=1/361. The same procedure adopted by previous researchers is employed [16, 41] to do the fitting, i.e., using the data at small displacement to fit, and extend to include increasingly larger displacement. Just as expected, the *F-d* curve exhibits a nonlinear relationship, which is out of the description of the classical beam model, and the modified beam model shows excellent fitting results. Recall the results in Fig. 3(a), it is concluded that the presence of defects does insignificant influence to the nonlinear-elastic behavior of the NW. It is worthy to mention that, the nonlinearity of the *F-d* curve is arisen from the axial stretching and increases with the increase of displacement. In other words, when the bending displacement is relatively small (say *d* is smaller than half of the cross-section size), the stretching effect should be ignorable [41], in such circumstance, the classical beam model should still be suitable to describe the bending behavior of the NW, as revealed in Fig. 3(b).

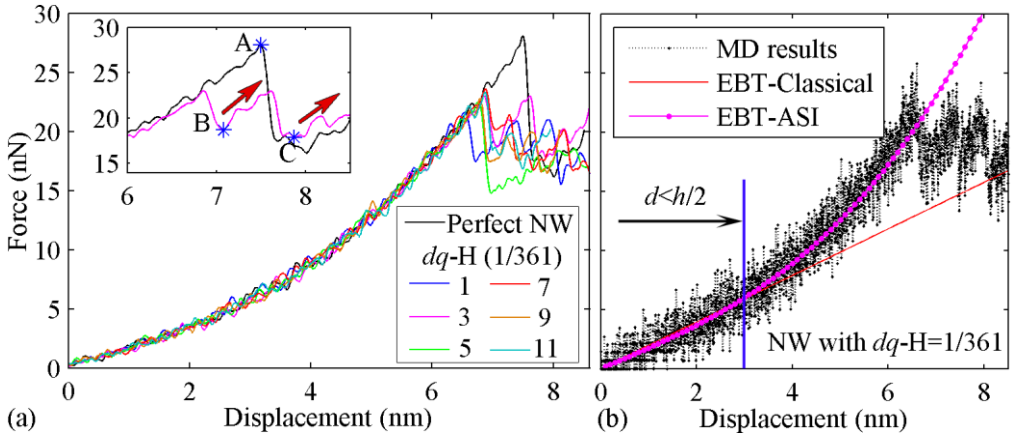


**Fig. 3.** (a) The *F-d* curves of NWs with different quantities of horizontal defects that located at the bottom surface. Inset figure enlarged the *F-d* curves of the perfect NW and the NW with *dq*-H=3/361 around the critical force. All curves are smoothed. (b) Comparisons between MD results and fitting results from EBT-Classical and EBT-ASI for the NW with *dq*-H=1/361.

Due to the similarity of the deformation process, only the perfect NW and the NW with *dq*-H=3/361 are compared in Fig. 4. Evidently, for the perfect NW, no dislocation is identified before the onset of yielding (Fig. 4(a)), which implies that the NW is under elastic deformation. When the displacement exceeds 7.51 nm (point 'A' in the inset of Fig. 3), partial dislocations begin to nucleate. From Fig. 4(b), the active nucleation and propagation of partial dislocations have generated a great amount of intrinsic stacking faults (iSFs). This deformation process continues at the bending displacement of 8.41 nm as illustrated in Fig. 4(c). For the NW with *dq*-H=3/361, the perfect crystal structure retained at the beginning, indicating an initial elastic deformation (Fig. 4(d)). The increase of the displacement finally leads to the yielding of the NW. From Fig. 4(e), two Shockley partial dislocations are found to intersect with each other, and with the NW's bottom and side surfaces simultaneously, which induce the formation of a stair-rod dislocation and a Lomer-Cottrell (LC) lock from the dislocations reaction [52] $a/6[1\bar{1}2]+a/6[1\bar{1}\bar{2}]=a/3[1\bar{1}0]$ (LC-h1). The Lomer-Cottrell lock has provided a strong barrier to the further glide of the dislocations on the two corresponding slip planes, which hardens the NW. As pointed out in the inset of Fig. 3 (point 'B'), the force exhibits a resumption process. From Fig. 4(f), another stair-rod dislocation ($a/3[110]$) and Lomer-Cottrell lock (LC-h2) is formed with further loading, which results the second hardening process (point 'C' in the inset of Fig. 3). Meanwhile, the intrinsic stacking fault (iSF) in Fig. 4(e) (iSF-b1) is vanished, which signifies the occurrence of full dislocations. Apparently, the plastic deformation of either the perfect NW or the NW with *dq*-H=3/361 is dominated by the nucleation and propagation of partial dislocations, and the existences of both iSF and extrinsic stacking fault (eSF) are observed for the defected NW (*dq*-H=3/361).

In-depth inspection of the plastic deformation of all NWs reveals that, the formations of the stair-rod dislocations and Lomer-Cottrell lock not only existed in the perfect NW (Fig.s 4(b) and (c)), but also

existed in other defected NWs. Hence, it is concluded that, the existences of these structures have thwarted attempts of the NW from an early yielding, which leads to the phenomenon that more defects does not necessarily mean a lower critical force. Additionally, for the defected NWs, it is found that the dislocation embryo initiates from the locations of the defects.

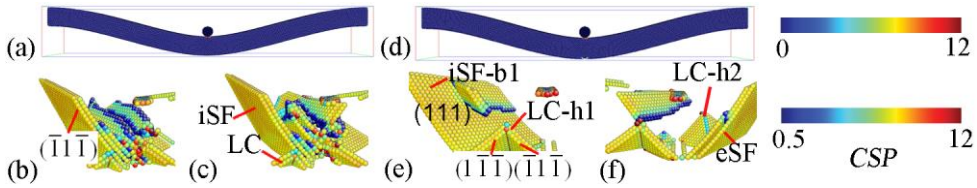


**Fig. 4.** Atomic configurations of NWs. Perfect NW: (a) *d*=7.51 nm; (b) *d*=7.81 nm; (c) *d*=8.41 nm; NW with *dq*-H=3/361: (d) *d*=6.90 nm; (e) *d*=6.99 nm; (f) *d*=7.87 nm. Atoms with their *CSP* value between 0 and 12 are viewed in figures a and d. Other figures are colored with *CSP* between 0.5 and 12, which only reveals the part with plastic deformation.

*3.2 Influence of defect's orientation*

Different orientations of the defect are then considered. Fig. 5 compares the *F-d* curves of NWs with *dq*-H=3/361, *dq*-V=3/361, *dq*-T=3/361 and *dq*-E=3/361. Evidently, all NWs share almost an identical *F-d* curve before yielding, and a notable reduction of the critical force is observed for all defected NWs, except the NW with an edge defect (*dq*-E=3/361).

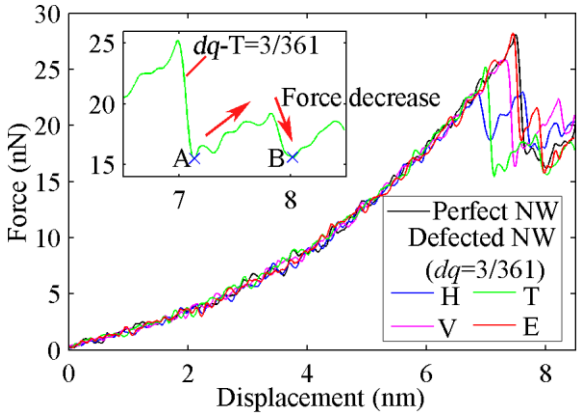


**Fig. 5.** The *F-d* curves of NWs with different orientated defects that located at the bottom surface. Inset figure enlarged the *F-d* curve of the NW with *dq*-T=3/361 around the critical force. All curves are smoothed.

The snapshots of the NW with *dq*-T=3/361 at different displacements are presented in Fig. 6. As is seen, the crystal structure of the NW remains unchanged before yielding. As illustrated in Fig. 6(b), a relatively large stair-rod dislocation and Lomer-Cottrell lock (LC-A) are firstly formed, which contributes to the resumption of force at the displacement around 7.14 nm (point 'A' in the inset of Fig. 5). However, this lock appears not effective enough to prevent the further movement of dislocations. From Fig. 6(c), LC-A is vanished due to the increasing load from the tip, and a smaller lock (LC-B) is formed. This process is reflected by the load decrease event as pointed out in the inset of Fig. 5.

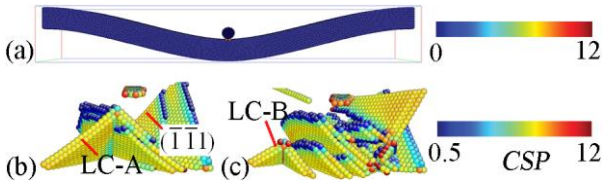


**Fig. 6.** Atomic configurations of the NW with *dq*-T=3/361. (a) *d*=7.02 nm; (b) *d*=7.14 nm; (c) *d*=8.03 nm. Atoms with their *CSP* value between 0 and 12 are viewed in figure a. Other figures are colored with *CSP* between 0.5 and 12, which only reveals the part with plastic deformation.

*3.3 Influence of defect's location*

The defects of *dq*-H=3/361, *dq*-V=3/361 and *dq*-T=3/361 that located at the NW's side surface (the surface parallel to the bend direction) and top surface (the surface underneath the tip) are also investigated. Again, all *F-d* curves are almost overlapped with each other before yielding. As seen in Fig. 7, the critical force has received an obvious reduction for NWs with the *dq*-H=3/361 and *dq*-T=3/361 on the side surface. Most interestingly, *F-d* curves of the NWs with defects on the top surface (*dq*-V and *dq*-T) almost overlap with the perfect NW, indicating an insignificant influence induced by the defects, and a hardening phenomenon is even observed for the NW with *dq*-H=3/361 on the top surface.

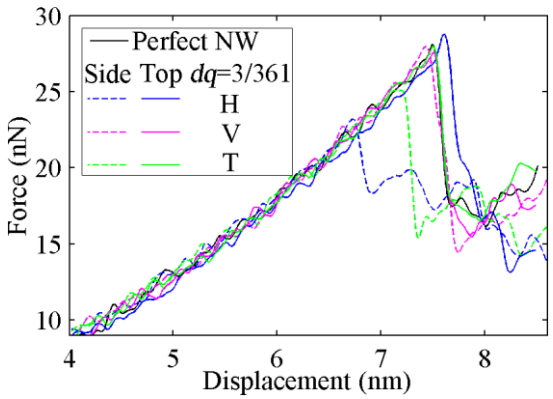


**Fig. 7.** The *F-d* curves of NWs with defects on the side and top surfaces. All curves are truncated at the displacement of 4 nm. All curves are smoothed.

Basically, all six defected NWs appear similar deformation mechanisms as the perfect NW, i.e., NW deforms elastically before yielding, the major deformation is achieved by the nucleation and propagation of partial dislocations, and the formations of stair-rod dislocations and Lomer-Cottrell lock are emerged.

*3.5 Comparisons and discussions*

Since the presence of defects might affect both NW's Young's modulus and moment of inertia, thus, the effective flexural rigidity (*EI*)* is taken as an parameter to assess the influence from different defects. As is seen, due to the term of the effective extensional rigidity (*EA*)*, the effective flexural rigidity is unable to be isolated from equation (3). Therefore, equation (2) is employed to conduct the

estimation of $(EI)^*$ by considering bending displacements that is smaller than half of the cross-section size (i.e., $d<h/2$). Fig. 8(a) depicts the changing pattern of the relative flexural rigidity $R_{EI}$ due to the different pre-existing defects on the NW's bottom surface. $R_{EI}$ is defined as the ratio of the effective flexural rigidity between the defected NW and the perfect NW, i.e., $R_{EI} = (EI)_d^* / (EI)_p^*$. It is found that, the presence of the pre-existing defects does not always lead to a weakening effect to the NW flexural rigidity. For NWs with *dq*-H equals 1/361, 5/361 and 9/361, an even enhanced flexural rigidity ($R_{EI}>1$) is observed. In the meanwhile, the increase of the defect quantity also doesn't mean an increasing reduction to the flexural rigidity, e.g., for the NW with *dq*-H equals 3/361, $R_{EI}$ is estimated around 0.9634, while a larger $R_{EI}$ about 0.9974 is found for the NW with *dq*-H equals 11/361. For the same defect quantity, the horizon defect is found to induce the largest reduction, followed by the edge defect and then the vertical defect. Specifically, an enhanced flexural rigidity is observed for the NW with a tilt defect.

Fig. 8(b) illustrates the influences from three different orientated defects (*dq*-H, *dq*-V, *dq*-T) when they are introduced to different surfaces. It is uniformly found that, the horizontal defect induces the largest weakening effect, followed by the vertical defect, and then the tilt defect. Particularly, the tilt defects located on all three surfaces even show a positive influence to the flexural rigidity. Just as expected, the defects on the surface that parallels to the bend direction (side surface) exert less influence to the flexural rigidity than the defects on the surface that perpendicular to the bending direction (bottom and top surfaces). In summary, the influence on the flexural rigidity that induced by the pre-existing surface defects is insignificant (within ±4%). This result, in the other hand indicates that the Young's modulus is insensitive to the pre-existing defects, which is consistent with the results obtained under tension [26] by previous researchers.

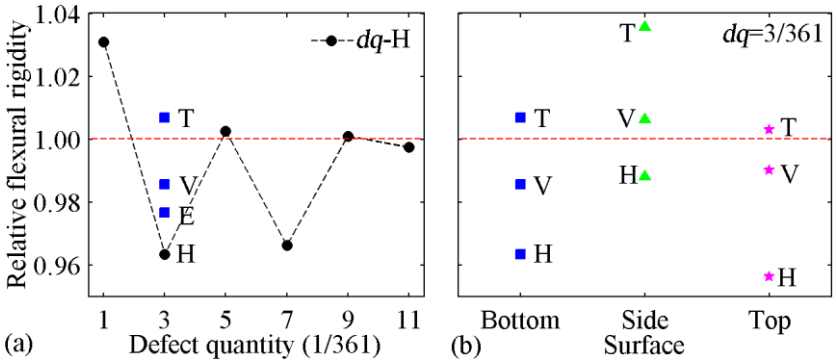


**Fig. 8.** Comparisons of the relative flexural rigidity ($R_{EI}$) between the perfect NW and defected NWs. (a) Defects located at the bottom surface; (b) Defects located at the bottom surface, side surface and top surface.

In the end, we compare the yield strength among different cases, which is calculated from equation (4). For the perfect NW, the yield strength is estimated as 13.11 GPa. Unlike the flexural rigidity, a relative large decrease of the yield strength is observed, as revealed in Fig. 9, e.g., the yield strength

of the NW with *dq*-H=1/361 is only around 10.08 GPa, which indicates a 23% reduction. As previously discussed, the reduction of the yield strength does not increase with the defect quantity. From Fig. 9(b), defects on the top surface exert the least effect to the yield strength, with the defects on the bottom surface cause the largest influence. The highest yield strength is found from the NW with *dq*-H=3/363 on the top surface.

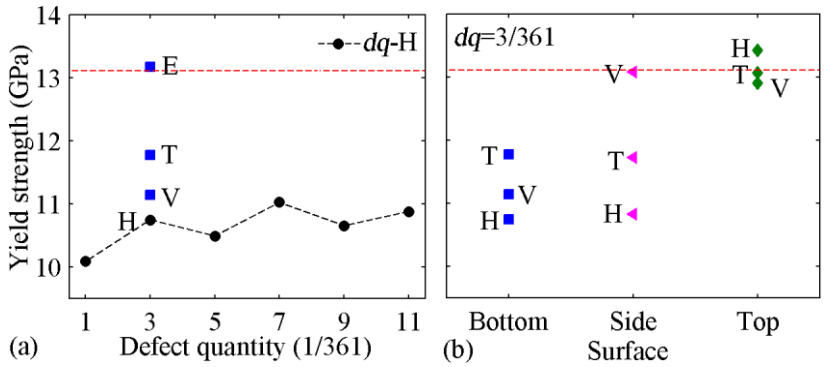


**Fig. 9.** Comparison of the yield strength (*Y*) between the perfect NW and defected NWs. (a) Defects located at the bottom surface; (b) Defects located at the bottom surface, side surface and top surface.

## 4. Conclusions

Based on the large-scale MD simulation, the classical Euler-Bernoulli theory and the modified Euler-Bernoulli beam model (augmented with a comprehensive consideration of surface/intrinsic effect and axial extension effect), the influence on the bending properties of Ag NWs from different pre-existing surface defects is thoroughly investigated. Considered NWs contain pre-existing surface defects either located at different surfaces (bottom, side and top surfaces), or with different orientations or with different quantities. Major conclusions include:

1) For the considered defects, the load-displacement (*F*-*d*) curves of different defected NWs appear almost consistent with the perfect NW before the onset of plastic deformation, which indicates the nonlinear-elastic deformation, as well as the flexural rigidity of the NW is insensitive to the surface defects;
2) Due to the presence of the defects, the yield strength received an evident decrease. Just as expected, the defects on the surface that perpendicular to the loading direction show larger influence than the defects on surfaces that parallel to the loading direction;
3) At the beginning of yielding, dislocation embryos initiate from the locations of the defects, and the plastic deformation is dominated by the nucleation and propagation of partial dislocations;
4) During the plastic deformation, the generation of stair-rod partial dislocations and Lomer-Cottrell lock are normally observed for all NWs under the considered temperature. The formation of these structures has thwarted attempts of the NW to an early yielding, which leads to the phenomenon that more defects does not necessarily mean a lower critical force.

**Acknowledgements**

Support from the ARC Future Fellowship grant (FT100100172) and the High Performance Computer resources provided by the Queensland University of Technology are gratefully acknowledged.

**References**

[1] A. Husain, J. Hone, H.W.C. Postma, X. Huang, T. Drake, M. Barbic, A. Scherer, M. Roukes, Appl. Phys. Lett., 83 (2003) 1240.
[2] M. Li, T.S. Mayer, J.A. Sioss, C.D. Keating, R.B. Bhiladvala, Nano Lett., 7 (2007) 3281-3284.
[3] D. Rugar, R. Budakian, H. Mamin, B. Chui, Nature, 430 (2004) 329-332.
[4] Y. Yang, C. Callegari, X. Feng, K. Ekinci, M. Roukes, Nano Lett., 6 (2006) 583-586.
[5] K. Eom, H.S. Park, D.S. Yoon, T. Kwon, Phys. Rep., 503 (2011) 115-163.
[6] Y. Yue, P. Liu, Z. Zhang, X.D. Han, E. Ma, Nano Lett., 11 (2011) 3151-3155.
[7] J.H. Seo, Y. Yoo, N.Y. Park, S.W. Yoon, H. Lee, S. Han, S.W. Lee, T.Y. Seong, S.C. Lee, K.B. Lee, P.R. Cha, H.S. Park, B. Kim, J.P. Ahn, Nano Lett., 11 (2011) 3499-3502.
[8] Y. Zhu, Q. Qin, F. Xu, F. Fan, Y. Ding, T. Zhang, B.J. Wiley, Z.L. Wang, Phys. Rev. B, 85 (2012) 045443.
[9] G. Richter, K. Hillerich, D.S. Gianola, R. Mo nig, O. Kraft, C.A. Volkert, Nano Lett., 9 (2009) 3048-3052.
[10] H.S. Park, J.A. Zimmerman, Phys. Rev. B, 72 (2005) 54106.
[11] J. Diao, K. Gall, M.L. Dunn, J. Mech. Phys. Solids, 52 (2004) 1935-1962.
[12] H.F. Zhan, Y.T. Gu, C. Yan, X.Q. Feng, P. Yarlagadda, Comput. Mater. Sci., 50 (2011) 3425-3430.
[13] P.A.T. Olsson, H.S. Park, Acta Mater., 59 (2011) 3883–3894.
[14] S. Jiang, H. Zhang, Y. Zheng, Z. Chen, J. Phys. D: Appl. Phys., 42 (2009) 135408.
[15] P. Olsson, S. Melin, C. Persson, Phys. Rev. B, 76 (2007) 224112.
[16] H.F. Zhan, Y.T. Gu, Comput. Mater. Sci., 55 (2012) 73-80.
[17] H.F. Zhan, Y.T. Gu, J. Appl. Phys., 111 (2012) 124303-124309.
[18] H. Zhan, Y. Gu, H.S. Park, Nanoscale, 4 (2012) 6779-6785.
[19] H.F. Zhan, Y.T. Gu, J. Phys. D: Appl. Phys., 45 (2012) 465304-465313.
[20] T.H. Kim, X.G. Zhang, D.M. Nicholson, B.M. Evans, N.S. Kulkarni, B. Radhakrishnan, E.A. Kenik, A.P. Li, Nano Lett., 10 (2010) 3096-3100.
[21] F. Sansoz, H. Huang, D.H. Warner, JOM Journal of the Minerals, Metals and Materials Society, 60 (2008) 79-84.
[22] M.J. Chen, G.B. Xiao, J.X. Chen, C.Y. Wu, SCIENCE CHINA Technological Sciences, 53 (2010) 3161-3167.
[23] E. Kuramoto, K. Ohsawa, T. Tsutsumi, CMES- Computer Modeling in Engineering and Sciences, 3 (2002) 193-200.
[24] Y. Zhang, H. Huang, S.N. Atluri, CMES: Computer Modeling in Engineering & Sciences, 35 (2008) 215-226.
[25] B. Wu, A. Heidelberg, J.J. Boland, J.E. Sader, X.M. Sun, Y.D. Li, Nano Lett., 6 (2006) 468-472.
[26] H.F. Zhan, Y.T. Gu, CMES: Computer Modeling in Engineering & Sciences, 80 (2011) 23-56.
[27] H.F. Zhan, Y.T. Gu, C. Yan, P.K.D.V. Yarlagadda, Adv. Mat. Res., 335 (2011) 498-501.
[28] H. Zhan, Y. Gu, P.K.D.V. Yarlagadda, C. Yan, in: 2012 12th IEEE Conference on Nanotechnology (IEEE-NANO), 2012, pp. 1-5.
[29] S. Plimpton, J. Comput. Phys., 117 (1995) 1-19.
[30] B. Wu, A. Heidelberg, J.J. Boland, Nat. Mater., 4 (2005) 525-529.
[31] A. Voter, Los Alamos Unclassified Technical Report LA-UR, (1993) 93-3901.
[32] H.S. Park, C. Ji, Acta Mater., 54 (2006) 2645-2654.
[33] R. Smith, C. Nock, S. Kenny, J.J. Belbruno, M. Di Vece, S. Palomba, R. Palmer, Phys. Rev. B, 73 (2006) 125429.
[34] W.G. Hoover, Phys. Rev. A, 31 (1985) 1695-1697.
[35] S. Nosé, J. Chem. Phys., 81 (1984) 511.
[36] C.L. Kelchner, S.J. Plimpton, J.C. Hamilton, Phys. Rev. B, 58 (1998) 11085-11088.
[37] M. Doyama, Nuclear Instruments and Methods in Physics Research Section B: Beam Interactions with Materials and Atoms, 102 (1995) 107-112.
[38] S. Tyagi, J. Lee, G. Buxton, A. Balazs, Macromolecules, 37 (2004) 9160-9168.
[39] W.J. Chang, Microelectron. Eng., 65 (2003) 239-246.
[40] S.P. Timoshenko, J.M. Gere, Theory of elastic stability, McGraw-Hill, New York, 1961.

[41] A. Heidelberg, L.T. Ngo, B. Wu, M.A. Phillips, S. Sharma, T.I. Kamins, J.E. Sader, J.J. Boland, Nano Lett., 6 (2006) 1101-1106.
[42] J. Diao, K. Gall, M.L. Dunn, Nat. Mater., 2 (2003) 656-660.
[43] H.S. Park, Nano Lett., 6 (2006) 958-962.
[44] W. Liang, M. Zhou, F. Ke, Nano Lett., 5 (2005) 2039-2043.
[45] H.S. Park, K. Gall, J.A. Zimmerman, Phys. Rev. Lett., 95 (2005) 255504.
[46] H. Liang, M. Upmanyu, H. Huang, Phys. Rev. B, 71 (2005) 241403.
[47] J. Diao, K. Gall, M. Dunn, J. Zimmerman, Acta Mater., 54 (2006) 643-653.
[48] H.F. Zhan, Y.T. Gu, J. Appl. Phys., 111 (2012) 084305.
[49] G. Wang, X. Feng, Appl. Phys. Lett., 94 (2009) 141913.
[50] R. Miller, V. Shenoy, Nanotechnology, 11 (2000) 139.
[51] V.B. Shenoy, Phys. Rev. B, 71 (2005) 094104.
[52] J.P. Hirth, J. Lothe, John Wiley and Sons, Inc., 1982, (1982) 857.